Journal of
Synchrotron
Radiation

ISSN 0909-0495

Received 18 April 2005
Accepted 14 July 2005

Advances in array detectors for X-ray diffraction techniques

Quentin S. Hanley[a,b] and M. Bonner Denton[c]*

[a]Department of Biological and Chemical Sciences, University of the West Indies, Cave Hill Campus, St Michael, Barbados, [b]School of Biomedical and Natural Sciences, Nottingham Trent University, Clifton Lane, Nottingham NG11 8NS, UK, and [c]Department of Chemistry, University of Arizona, PO Box 210041, Tucson, AZ 85721, USA. E-mail: mbdenton@u.arizona.edu

Improved focal plane array detector systems are described which can provide improved readout speeds, random addressing and even be employed to simultaneously measure position, intensity and energy. This latter capability promises to rekindle interests in Laue techniques. Simulations of three varieties of foil mask spectrometer in both on- and off-axis configurations indicate that systems of stacked silicon detectors can provide energy measurements within 1% of the true value based on the use of single 'foils' and ~10000 photons. An eight-detector hybrid design can provide energy coverage from 4 to 60 keV. Energy resolution can be improved by increased integration time or higher flux experiments. An off-axis spectrometer design in which the angle between the incident beam and the detector system is 45° results in a shift in the optimum energy response of the spectrometer system. In the case of a 200 μm-thick silicon absorber, the energy optimum shifts from 8.7 keV to 10.3 keV as the angle of incidence goes from 0 to 45°. These new designs make better use of incident photons, lower the impact of source flicker through simultaneous rather than sequential collection of intensities, and improve the energy range relative to previously reported systems.

Keywords: CCD; CID; CMOS; Laue diffraction; spectrometer.

1. Introduction

Array-detector-based camera systems and, in particular, charge-coupled-device (CCD) cameras have had a major impact on X-ray diffraction techniques. These systems allow simultaneous observation of X-ray diffraction patterns over a reasonably large area.

Today's systems have evolved from using small CCDs into modern detectors using relatively large CCDs (4 K × 4 K pixel formats), often coupled to a fiber optic minifier (a fiber bundle drawn out on one end which effectively captures a larger image and reduces its size to that of the smaller CCD). The glass in the minifier also serves to shield the relatively delicate CCD from X-rays. If the CCD is directly exposed to a high X-ray flux, serious degradation of its performance will rapidly occur. Such CCD/CCD-minifier 'cameras' observe light produced by the incident X-rays in a diffraction pattern when they impinge on a phosphor screen. While these systems have greatly speeded up the acquisition of X-ray diffraction pattern information in many applications, current CCD cameras still limit the inherent capabilities of some experimental situations. Notably, experiments using synchrotrons as an X-ray source could be more efficient if the time spent reading the information from the CCD could be significantly reduced, or if alternative approaches to pattern generation and observation were realised (in particular, Laue methods).

This manuscript reviews concepts presented at the 'COMPRES Workshop on Structure Determination at a Megabar,' held at Argonne National Laboratory, 13–14 November 2004, covering advances in CCD architecture, random pixel addressing in charge-injection devices (CIDs), complementary metal oxide semiconductors (CMOS) and CMOS photodiode arrays, as well as methods for implementing Laue diffraction techniques with available device technology. The purpose of this manuscript is to generate interest and discussion leading toward improved camera technologies.

1.1. Overview of array detectors

The standard architecture for today's CCDs is shown in Fig. 1(*a*). Light is converted into charge and stored as electrons within 'pixels'. Readout is accomplished by gating off the light source (in this case, X-rays impinging on the visible-light-generating phosphor) and shifting charge within the horizontal parallel registers one pixel to the right (as drawn). This process 'loads' the charge contained in the most right-hand pixels in each parallel register into the serial register. The

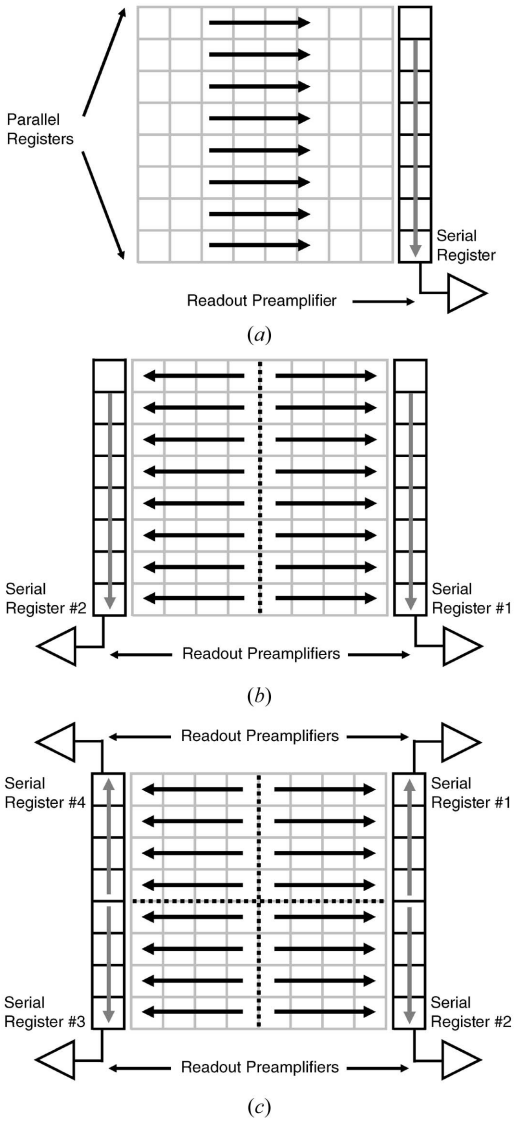

Figure 1
(*a*) Single readout port CCD showing horizontal clocking in the parallel registers and vertical clocking in the serial register. (*b*) A two-port readout architecture. Charge packets are shifted simultaneously, but in opposite directions from the parallel registers, into two serial registers. With a given read rate, this reduces full frame readout time by a factor of two. (*c*) A four-port readout architecture. Note that four full sets of analog and analog-to-digital converters must be used in parallel, significantly increasing the cost of the support electronics.

charge packets in the serial register are next clocked vertically down and subsequently 'read' by the readout preamplifier. After the entire string of pixel information is read out of the serial register, the horizontal registers are again clocked reloading the serial register. This entire process is repeated until all of the charge packets have been clocked out of the parallel registers and the serial register has been fully read out.

The factors limiting readout speed are the rate of clocking the serial register and, more importantly, the rate of reading and resetting the readout preamplifier. Faster readout speeds generally increase the noise associated with the readout process.

Major research efforts are underway in a number of laboratories exploring means of increasing the readout (clock) rate while maintaining low readout noise levels. As improvements are realised, they are being rapidly incorporated into commercially available CCDs.

A number of other techniques to increase the effective readout speed (reduce the time to read the entire frame) are being utilized to speed up current CCD technology. These include binning, *i.e.* the process of clocking charge contained in two or more pixels into one serial register location (horizontal binning as drawn), or two or more packets in the serial register into the readout amplifier node (vertical binning as drawn). This in effect reduces the total number of charge packets which must be read by the readout preamplifier, albeit at a cost of reduced spatial resolution. Horizontal and vertical binning are often used together to further reduce the total number of charge packets in a complete frame while introducing a symmetrical loss in spatial resolution.

Improved readout speed of either $\times 2$ or $\times 4$, with no loss in resolution or increased readout noise, is also possible through splitting the CCD in half (Fig. 1*b*) or in quarters (Fig. 1*c*) and simultaneously reading the smaller portions of the CCD (Sims, 1994). This scheme does require additional readout electronics (analog train and analog-to-digital converters), substantially increasing the cost of the entire camera systems.

A spin on this approach has been investigated initially by Mark Wadsworth, then at Jet Propulsion Laboratories, and subsequently by Eugene Atlas and Wadsworth at Imager Laboratories, San Marcos, CA, USA, and Tangent Technologies, Monrovia, CA, USA (Atlas & Wadsworth, 2003). This hybrid imager technology (HIT) combines the best features of scientific CCDs with a special CMOS readout circuit, which provides improved high-gain preamplifiers, charge mode (capacitive transimpedance) amplifiers, and the ability to practically implement a large number of readout trains on a single integrated circuit die. This is a practical way of increasing the total number of regions being read in parallel without substantially adding to the cost of the camera systems.

Construction of the hybrid device involves bump bonding a properly configured (broken up into a large number of segments) high-performance CCD on top of the CMOS readout circuitry. This 'stack' is then mounted in a conventional integrated circuit package. The indium bump bonding technique allows practical implementation of the large number of interconnects while maintaining low spurious capacitances (see Fig. 2).

Increasing the number of parallel channels to 64, 128, or even 512, with a 1 MHz pixel read rate allows reduction of frame acquisition from 16 s with a single port read device on a 4 K $\times$ 4 K CCD to 31.25 milliseconds with a 512 channel device (Fig. 3). Other unique features allow an increase in attainable signal to noise.

Another feature of the device in Fig. 3 is that, since frame transfer registers are used, parallel readout of a captured frame can be implemented while the next data set is being acquired. This feature eliminates some, or all, of the dead time for reading data from a CCD encountered with many

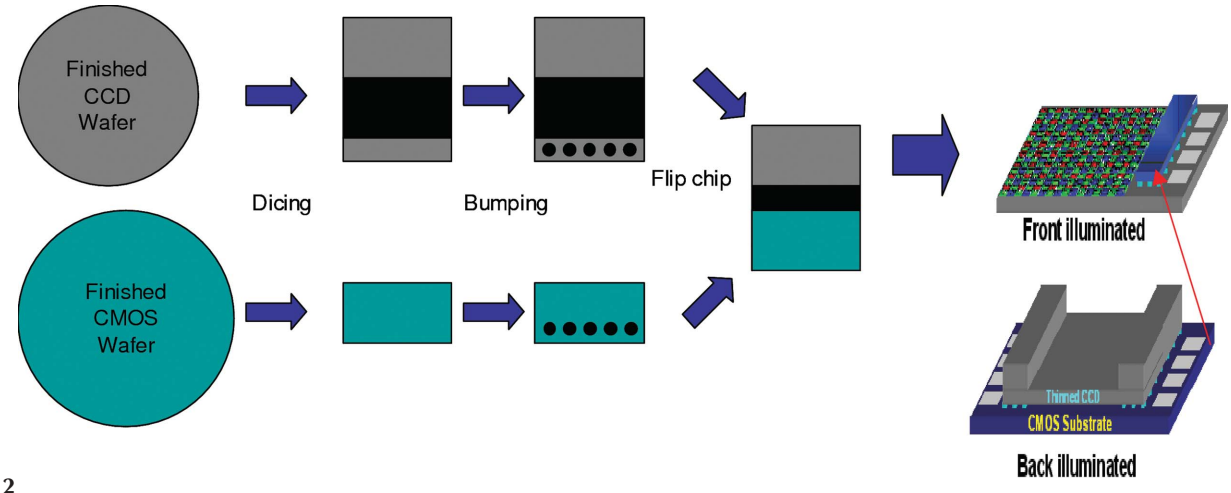

Figure 2
HIT fabrication diagram. A hybrid imaging technology device combines the best characteristics of CMOS and CCD devices. Multiple conventional 'small' high-performance CCD devices are fabricated on a single die. Separately, multiple readout channels are produced using CMOS technology. The two finished devices are bump bonded together (one 'flipped' on top of the other) to produce the final hybrid system capable of reading all of the 'small' CCD segments in parallel.

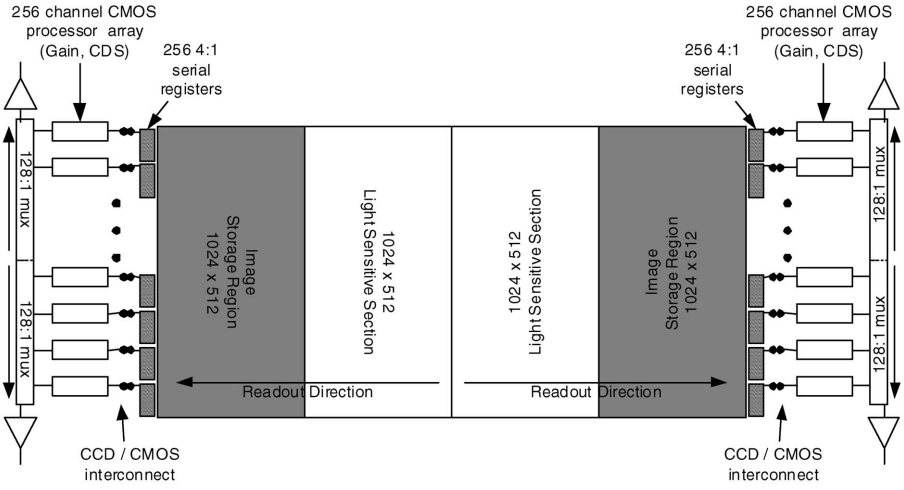

Figure 3
Conceptual schematic of a 1024 × 1024, 512 channel, split frame transfer HIT sensor.

conventional devices. Of course, frame storage registers can be, and have been, implemented in conventional CCDs. However, in cases where the data readout time greatly exceeds the data acquisition time, the saving in time *versus* added cost becomes of little value.

Two other types of devices, the CID and CMOS array sensors, offer intriguing characteristics for certain applications. Unlike CCDs, both of these classes of devices can be configured with random addressing and non-destructive readout (NDRO) capabilities. Random addressing allows high-speed 'jumping' between two or more pixels or pixel sub-arrays without having to at least clock through all other pixels, as in a conventional CCD. This mode could be useful for following kinetics of structure change (such as in a pressure jump or drop experiments). NDRO mode allows the device to be read out while an exposure (integration) is taking place. Overall, intra-image dynamic range can be increased by measuring very bright pixels and then rapidly resetting them to zero charge before the charge level in that pixel reaches a non-linear region.

Dimly illuminated pixels are allowed to continually integrate until they provide an NDRO signal sufficiently above the detection limit to satisfy the criteria of the experiment (Sims & Denton, 1990). This process, termed random access integration (RAI) (Pilon *et al.*, 1990), allows the course of the exposure to be monitored while greatly extending the upper dynamic range for the brightest illuminated pixels. Even when not using RAI mode, most CID and CMOS imagers do not suffer from blooming problems encountered at very high light levels with many CCDs (note anti-blooming drains can be incorporated in a CCD's design with a modest loss in fill factor, *i.e.* the region of the pixel containing the anti-blooming drain is not sensitive to photons).

An interesting new CMOS array design has recently been introduced by Rad-icon Imaging Corp, Santa Clara, CA, USA. These devices incorporate an on-chip phosphor and are capable of direct detection of X-rays. They are being marketed for industrial X-ray imaging and can be purchased with support electronics suitable for evaluating the technology. These devices are relatively resistant to degradation as a result of sustained direct exposure to X-rays, particularly to white-light X-rays below 45 keV. Additionally, radiation degradation is manifested in an increase in dark current. Since these devices, as well as many other silicon devices, demonstrate a factor of two reduction in dark current for every 8 K they are cooled, refrigerating these devices to 77 K will greatly extend the useful exposure time.

These in-beam X-ray detecting devices suggest an interesting new approach for measuring position, intensity and

energy necessary for the optimal application of Laue X-ray methods.

1.2. Laue diffraction revisited

The Laue experiment differs from the traditional X-ray diffraction experiment by the use of a polychromatic or 'white' X-ray beam. The multiple wavelengths give rise to a diffraction pattern characterized by (*a*) higher spot density than in monochromatic experiments owing to a more expansive view of reciprocal space, (*b*) diffraction spots created by X-rays of varying energy, (*c*) a subset of spots which are created by overlapping orders of diffraction. This set of properties has been a source of great interest in the technique while at the same time making it difficult to implement.

The Laue experiment remains a challenge to instrumentation designers and widespread use of the Laue method has been restricted owing to harmonic overlap, limited capacity to measure accurate unit cells, limited ability to assign space groups, and systematic under-representation of low-frequency information (Helliwell, 1992; Cassetta *et al.*, 1993; Amoros *et al.*, 1975). Despite considerable success in applying the Laue method to the analysis of proteins (Yamashita *et al.*, 2003; Stoddard & Farber, 1995), it is rarely, if ever, used as a standalone method for structure determination. Rather, it is more often used in tandem with monochromatic methods to provide high-speed 'snapshots' of perturbations to known structures. While progress has been made on all aspects of the Laue problem, further progress is needed to develop the full potential of the method.

One approach to unscrambling harmonics, determining units cells and assigning space groups is a system of calibrated absorbers allowing the energy of individual spots to be determined. One approach to this was a foil mask spectrometer system which was capable of determining small unit cells and assigning systematic absences to spots containing harmonic overlap (Hanley *et al.*, 1997). Separation of harmonic content of Laue diffraction spots has been treated in some detail both theoretically and experimentally (Hanley *et al.*, 1996, 1997) and will not be treated at length here. It is, however, likely that any improvements in foil mask spectrometers will improve the ability to separate harmonics. The availability of new imaging technologies having a combination of high speed, large well capacity, and large area in a potentially stackable format makes this approach to Laue diffraction worth revisiting.

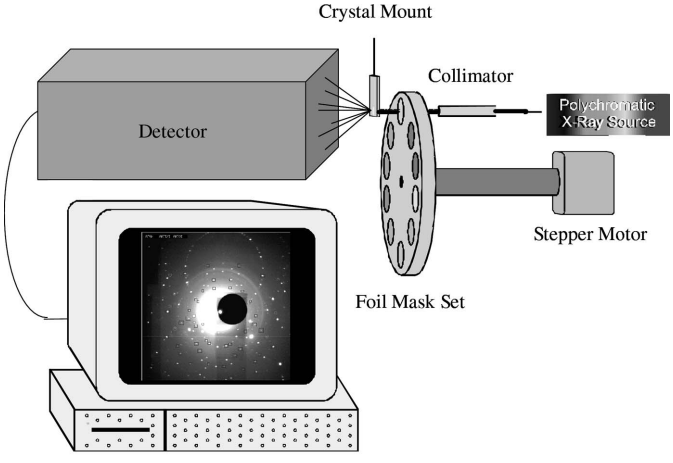

Figure 4
Block diagram of a type I spectrometer.

2. Definitions and theory

Four types of X-ray spectrometers for Laue diffraction will be considered here:

(i) A type I (Fig. 4) spectrometer is the type described by Hanley *et al.* (1996) and consists of a series of foils introduced into the X-ray beam prior to the crystal. An image is collected of the Laue pattern produced by the X-rays passing through each foil and the energies computed based on the known attenuation factors of the materials in the foil.

(ii) A type II spectrometer (Fig. 5) is one that works on the UNSCRAM principle described by Helliwell *et al.* (1989) in which a set of stacked calibrated absorbers is used to unscramble the overlapping orders of diffraction in a Laue pattern. The original UNSCRAM procedure used stacks of film in a film pack. With the exception of the lowermost film layer in the pack, each layer of film in the pack served as both a detector and a calibrated absorber. While these authors did not specifically describe a spectrometer, adapting the principle to measure the energies of single wavelength spots is straightforward. Similarly to the UNSCRAM procedure, detectors in the type II spectrometer serve dual roles as calibrated absorber and detector elements. A type II spectrometer will be referred to as heterogeneous when the calibrated absorbers are not of a single material.

(iii) A type III spectrometer is the same as the type I spectrometer except the foils are placed after the crystal.

(iv) A type IV spectrometer (Fig. 6) is a hybrid consisting of any combination of types I, II and III. Such a spectrometer is

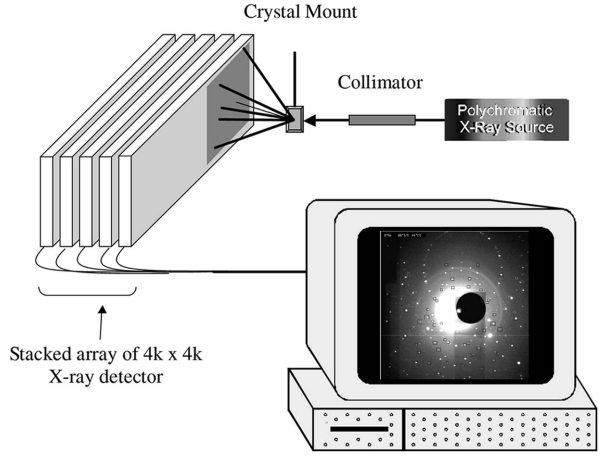

Figure 5
Block diagram of a type II spectrometer implemented with a stack of silicon-based array detectors. Note that the layers of the stacked array detectors serve a role as calibrated absorbers for subsequent layers.

advantageous for allowing extended energy ranges to be determined.

Type II, III and IV spectrometers are subject to an off-axis angle-dependent transmission efficiency according to

$$T = \exp[-\mu(\lambda)(x/\cos\theta)]. \quad (1)$$

In (1), $\mu(\lambda)$ is the linear absorption coefficient of the material at an X-ray wavelength λ, x is the thickness of the foil and θ is the angle of incidence of the X-rays creating a particular diffraction spot.

The error in energy determinations made using a calibrated absorber depend on the change in energy with transmission efficiency and number of X-ray photons observed (Hanley *et al.*, 1996),

$$\sigma_E = \left|dE/dT\right|\left[(1+T)T/I_0\right]^{1/2}. \quad (2)$$

In (2), σ_E is the error in the measured energy, $|dE/dT|$ is the material-dependent derivative of energy with respect to transmission efficiency, T is the transmission efficiency and I_0 is the intensity in the absence of any absorbers. The simulated error is conveniently presented as a percentage,

$$\sigma_E/E\,(\%) = 100\left\{\left|dE/dT\right|\left[(1+T)T/I_0\right]^{1/2}/E\right\}. \quad (3)$$

A simulated spectrometer will be said to have good energy resolution if the measured transmission is in the range 0.1–0.9 and has a predicted error of less than 1% when collecting 10000 X-ray photons.[1] It should be noted that this is the single absorber error. Combining the data from several absorbers or a system of absorbers should yield a better estimate.

3. Materials and methods

Simulations of transmission efficiency were based on data from the NIST X-ray Attenuation and Absorption for Materials of Dosimetric Interest (XAAMDI) database (Chantler *et al.*, 2005; Hubbell & Seltzer, 2004). The design range in the spectrometer simulations was from 4 to 60 keV. The silicon detectors were modeled on the Radeye8 (Rad-icon Imaging Corp, Santa Clara, CA, USA) CMOS photodiode arrays (98.4 mm × 98.4 mm).

4. Results and discussion

4.1. Type II spectrometer consisting of stacked two-dimensional diode arrays having a thickness of 200 micron

A silicon-based photodiode array detecting X-rays below a 200 µm-thick silicon slab results in transmission efficiencies ranging from less than 0.00001 at 4 keV to 0.98 at 60 keV (Fig. 7). Consequently, X-rays having energies below 6 keV can be assumed to be completely absorbed in the top array in the stack and those up to 9 keV will provide relatively poor estimates of the transmission efficiency. As a result, a type II spectrometer constructed of stacked 200 µm silicon photodiode arrays will be 'energy blind' up to approximately 9 keV. The system of stacked absorbers allows the *K*-edges of other absorbing materials to be resolved up to the design limit of 60 keV. When an X-ray signal of 10000 photons is assumed, the type II spectrometer has a useful energy range between 9 keV and 30 keV when the transmission efficiency (Fig. 7) and the estimated energy error are considered (Fig. 8).

An alternative approach using thinned silicon detectors was investigated to provide energy coverage down to 4 keV. These computations (not shown) indicated that the top device must be thinned to about 25 µm in order for this approach to be

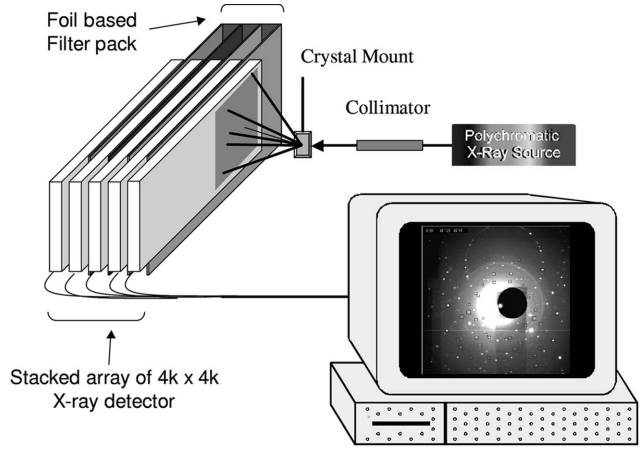

Figure 6
Hybrid spectrometer system implemented with a stacked array of two-dimensional area detectors and a foil pack. The foil packs can be made to be reconfigurable depending on experimental conditions.

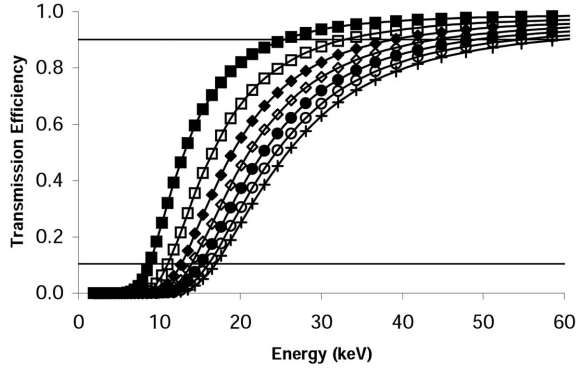

Figure 7
On-axis transmission efficiency response of a type II spectrometer constructed from eight stacked 200 µm-thick silicon photodiode arrays. This spectrometer can provide good measurements of energy between 9 and 25 keV and provide *K*-edge ambiguity resolution up to 60 keV. Curves show simulated transmission efficiency observed by the second (filled squares), third (open squares), fourth (filled diamonds), fifth (open diamonds), sixth (filled circles), seventh (open circles) and eighth (crosses) detector in the stack. These correspond to the signal observed through 200, 400, 600, 800, 1000, 1200 and 1400 µm of silicon. Not shown is the first diode array in the stack which provides the I_0 signal. Horizontal lines indicate the position of 0.1 and 0.9 on the transmission efficiency axis. Note: simulations neglect the absorption of dopants, passivating layers and electrode materials.

[1] The selection of 1% error and 10000 photons has been made arbitrarily and is for comparison purposes. It should be noted that errors in unit-cell dimensions do not scale exactly with the percent error in single foil energy measurements (Hanley *et al.*, 1997). This is due to spectrometers reporting energy based on several foils and unit-cell determinations being made based on multiple reflections.

practical. While thinned silicon-based imaging systems are widely available, they tend to be more costly than normal devices.

4.2. Type I spectrometer consisting of a set of aluminium foils

To mitigate the 'energy blind' region of the type II spectrometer described above, an investigation was made into the characteristics of an aluminium-based spectrometer system.

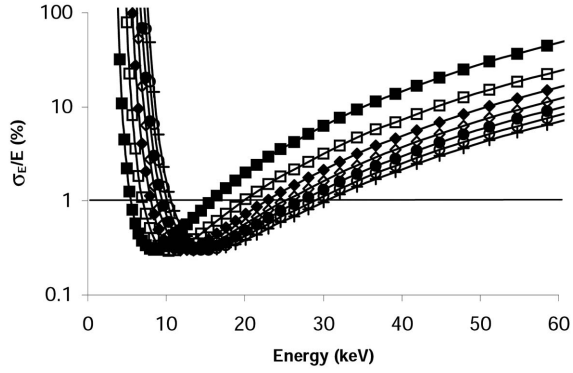

Figure 8
Predicted on-axis energy errors from a type II spectrometer constructed from eight stacked 200 μm-thick silicon photodiode arrays. While the predicted error first dips below 1% near 5.5 keV, the transmission efficiency at this energy is low (4×10^{-4}). The transmission efficiency limits the measurement until 9 keV. The spectrometer then provides good measurements of energy up to 30 keV and should allow *K*-edge ambiguities to be resolved up to 60 keV. Curves show predicted energy errors observed by the second (filled squares), third (open squares), fourth (filled diamonds), fifth (open diamonds), sixth (filled circles), seventh (open circles) and eighth (crosses) detector in the stack. These correspond to the signal observed through 200, 400, 600, 800, 1000, 1200 and 1400 μm of silicon. Not shown is the first diode array in the stack which provides the I_0 signal. Simulation corresponds to a detected signal consisting of 10000 X-rays. Note: simulations neglect the absorption of dopants, passivating layers and electrode materials.

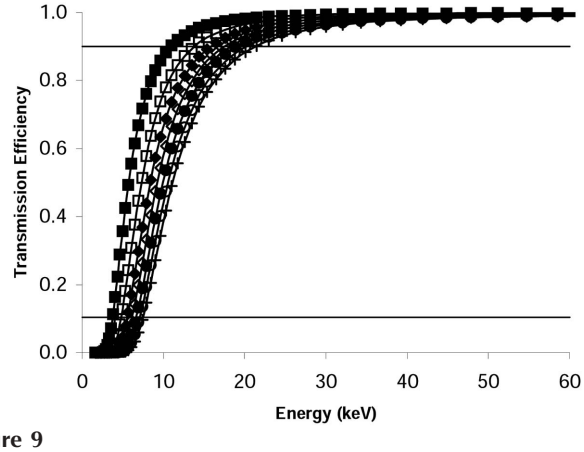

Figure 9
On-axis transmission efficiency response of a type I spectrometer constructed from stacked Al foils. This spectrometer can provide good measurements of energy between 4 and 15 keV. Curves show predicted transmission efficiencies observed by the first (filled squares), second (open squares), third (filled diamonds), fourth (open diamonds), fifth (filled circles), sixth (open circles) and seventh (crosses) detector in the stack. These correspond to the signal observed through 20, 40, 60, 80, 100, 120 and 140 μm of aluminium. Note: in contrast to the type II spectrometer, the I_0 signal is collected in the absence of a foil.

Owing to the high absorption of silicon at low energy, a type I or type III spectrometer is advisable for this region and the properties of aluminium made it a good candidate absorber. A spectrometer system consisting of seven Al foils of thickness 20, 40, 60, 80, 100, 120 and 140 μm removes the energy blind region between 4 and 9 keV (Figs. 9 and 10). When combined with the type II spectrometer (Figs. 7 and 8), good energy response is obtained from 3.9 to 30 keV. Almost all of the improvement below 9 keV can be achieved with the first (20 μm) and last (140 μm) foils. Using this reduced foil set, only two additional exposures must be made. Users of such a hybrid system will need to weigh the relative merits of the wider energy range *versus* either additional exposures or the higher cost of thinned silicon imaging devices.

4.3. Type I spectrometer consisting of Ag, W or Au foils

The stacked silicon type II detector system was shown to lose energy resolution above 30 keV. The use of the higher-atomic-mass elements silver (Ag), tungsten (W) and gold (Au) was investigated to determine which would be most efficient for creating a spectrometer capable of working above the limit of the silicon type II system (Fig. 11). For X-ray energies between 30 and 60 keV, the silver foils provide the best coverage. One disadvantage of silver is the prominent *K*-edge at 25.6 keV. When assembled into a spectrometer, it must be used together with other elements to properly assign the initial energy. Similar to the aluminium system, most of the improved energy range can be provided by two Ag foils (30 and 120 μm). This will provide good energy coverage over the entire range from 30 to 60 keV. Unlike the Al system, the Ag foils may be incorporated into a type II stack.

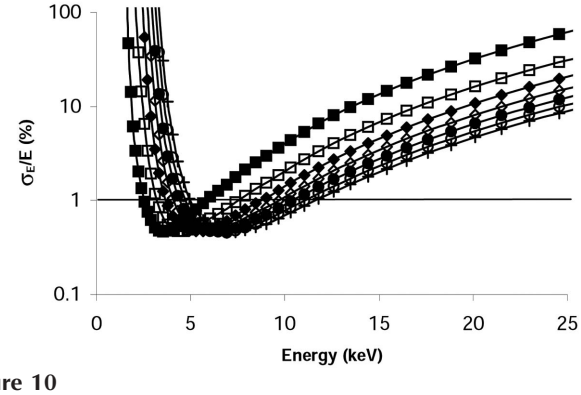

Figure 10
Energy errors from a type I spectrometer consisting of seven Al foils. While the predicted error first dips below 1% near 2.7 keV, the transmission efficiency is too small at this energy (4×10^{-4}). The transmission efficiency limits the measurement until 3.8 keV. The spectrometer then provides good measurements of energy up to 11 keV. Curves show predicted energy errors observed by the first (filled squares), second (open squares), third (filled diamonds), fourth (open diamonds), fifth (filled circles), sixth (open circles) and seventh (crosses) image in the series. These correspond to the signals observed through 20, 40, 60, 80, 100, 120 and 140 μm of aluminium. Simulation corresponds to a signal consisting of 10000 X-rays. Note: in contrast to the type II spectrometer, the I_0 signal is collected in the absence of a foil.

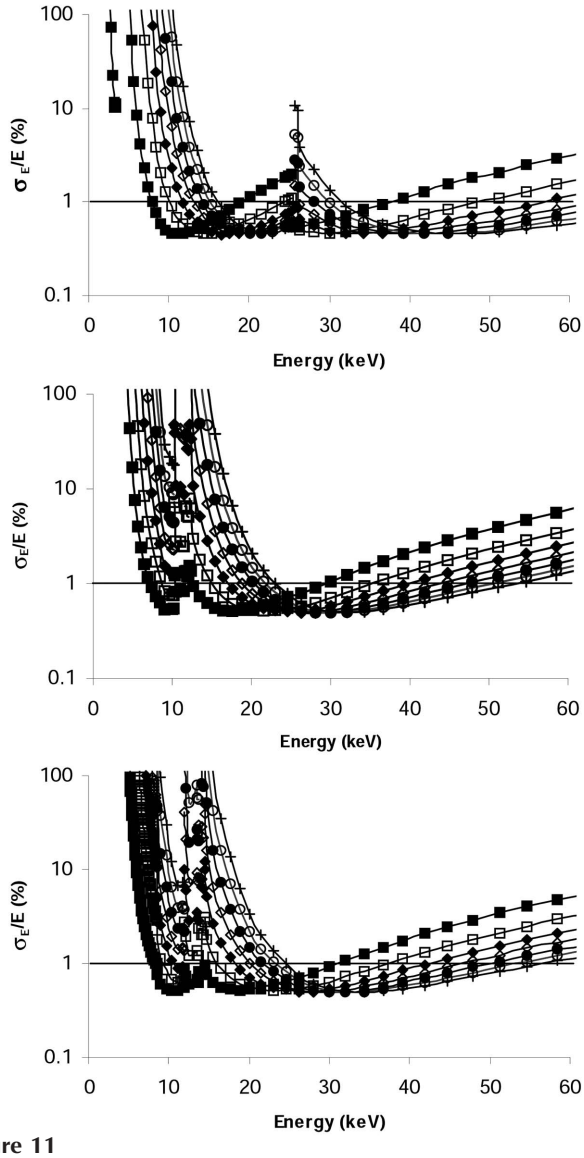

Figure 11
Error diagrams for type I spectrometers constructed using silver (top panel), tungsten (middle panel) and gold (bottom panel). The discontinuity in the top panel is due to the silver *K*-edge. Discontinuities in the W and Au data are due to *L*-edge effects. Of these elements, only silver is able to provide good energy measurements out to 60 keV. Au (*K*-edge 80 keV) and W (*K*-edge 69 keV) could be employed to good effect in spectrometers working up to 100 keV. Simulations all assume that I_0 is 10000. Silver simulation consists of 30 (filled squares), 60 (open squares), 90 (filled diamonds), 120 (open diamonds), 150 (filled circles), 180 (open circles) and 210 μm (crosses) foil thickness. Tungsten and gold simulations consist of 15 (filled squares), 25 (open squares), 35 (filled diamonds), 45 (open diamonds), 55 (filled circles), 65 (open circles) and 75 μm (crosses) foils.

4.4. Heterogeneous type II spectrometer

Based on the previous considerations, a heterogeneous type II spectrometer consisting of a stack of eight silicon-based detector systems was simulated. In this configuration, the top detector in the stack is thinned to 25 μm, the remaining seven are of normal 200 μm thickness. Between the fifth and sixth detector a 30 μm Ag foil is interposed, between the sixth and seventh a 50 μm Ag foil is introduced, and between the seventh and eighth an 80 μm Ag foil is used. This yields a spectrometer system with better than 1% error from slightly above 4 keV to 60 keV (Fig. 12).

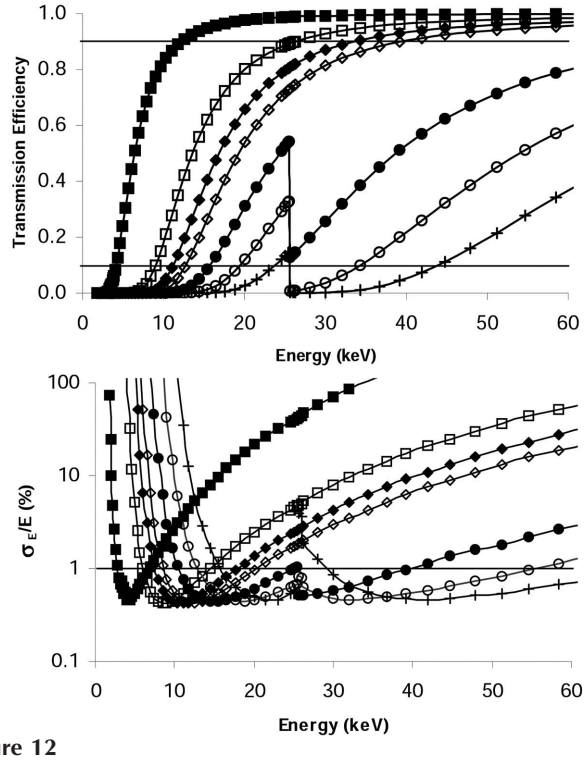

Figure 12
On-axis transmission efficiency and energy error of a heterogeneous type II spectrometer constructed from Si and Ag. This spectrometer can provide good measurements of energy between 4 and 60 keV. Curves show predicted energy errors observed by the second (filled squares), third (open squares), fourth (filled diamonds), fifth (open diamonds), sixth (filled circles), seventh (open circles) and eighth (crosses) detector in the stack. These correspond to the signal observed through 25 μm Si, 225 μm Si, 425 μm Si, 625 μm Si, 625 μm Si and 30 μm Ag, 825 μm Si and 80 μm Ag, and 1025 μm Si and 160 μm Ag.

4.5. Type II and type III off-axis behavior

Of the configurations considered, the heterogeneous type II spectrometer showed the best simulated response. As noted in the *Definitions and theory* section, type II, III and IV spectrometers are all subject to an angle-dependent response. For example, an X-ray beam passing through a 200 μm-thick silicon slab at an angle of 45° will be attenuated by a total of 283 μm of silicon. This shifts the minimum energy response of the spectrometer from about 8.7 keV up to 10.3 keV (not shown). While this is not a serious degradation of performance, it is significant and corrections after data collection will need to be applied.

5. Discussion

Foil mask spectrometers are highly specialized systems tailored to the specific problems encountered in Laue diffraction. They are designed to provide energy measurements of monochromatic diffraction spots. Standard texts describing the behavior of energy-dispersive and wavelength-dispersive measurements of X-ray energies indicate an accu-

racy of between 0.2 to 2.5% depending on the instrument and wavelength of interest (Strobel & Heineman, 1989). The 1% error presented as a target for comparison purposes should exceed the capabilities of energy-dispersive systems. Previous reports of foil mask spectrometer data gave results between ~15 keV and 30 keV (Hanley *et al.*, 1996). The stacked system described here should provide better performance over a wider range of energies. The simulations presented here on energy errors refer to single foil determinations. It is likely that determinations made in a stacked set of silicon detectors will exceed the capabilities of the previous approaches to measuring energies in monochromatic Laue spots. The new generation of large-area X-ray optimized CMOS photodiode arrays should revolutionize X-ray diffraction applications. Toward that goal a number of factors should be noted:

(i) A system of stacked detectors can be designed to have a dynamically reconfigurable set of foils. This will provide for several situations. The number of masks limits the number of harmonics that can be separated. In order to increase the capacity to assign space groups and include low-frequency information, additional masks can be introduced as needed. Further, a reconfigurable system of stacked detectors can be changed to match the energy requirements of a particular experiment.

(ii) The capability provided by the Ag foils in the heterogeneous type II spectrometer could also be introduced by a phosphor. Additionally, it is likely that the response to higher energies will need to be enhanced by the use of phosphors since only a small fraction will be absorbed in the silicon device.

6. Conclusion

Most array detectors employed today in X-ray crystallography are general purpose devices which have been adapted for their role in X-ray, often by the use of phosphor X-ray to visible light converters and/or fiber optic minifiers.

New generations of devices designed for direct detection of X-rays, or with characteristics specifically engineered for X-ray applications, are currently under development or are awaiting funding for development. Such detectors hold great promise for advancing the field of X-ray crystallography.

The authors would like to thank Eugene Atlas and Mark Wadsworth, Imager Laboratories; Gary Sims, Spectral Instruments; and Gene Weckler, Rad-icon Imaging Corp.

References

Amoros, J. L., Buerger, M. J. & Canut de Amoros, M. (1975). *The Laue Method.* New York: Academic Press.

Atlas, G. & Wadsworth, M. V. (2003). *Proc. SPIE*, **5167**, 121–126.

Cassetta, A., Deacon, A., Emmerich, C., Habash, J., Helliwell, J. R., McSweeney, S., Snell, E., Thompson, A. W. & Weisgerber, S. (1993). *Proc. R. Soc. London A*, **443**, 177–192.

Chantler, C. T., Olsen, K., Dragoset, R. A., Kishore, A. R., Kotochigova, S. A. & Zucker, D. S. (2005). *X-ray Form Factor, Attenuation and Scattering Tables*, Version 2.1, http://physics.nist.gov/ffast (25 March 2005). National Institute of Standards and Technology, Gaithersburg, MD. Originally published as Chantler, C. T. (2000). *J. Phys. Chem. Ref. Data*, **29**, 597–1048 and Chantler, C. T. (1995). *J. Phys. Chem. Ref. Data*, **24**, 71–643.

Hanley, Q. S., Campbell, J. W. & Denton, M. B. (1997). *J. Synchrotron Rad.* **4**, 214–222.

Hanley, Q. S., Dunphy, D. & Denton, M. B. (1996). *J. Synchrotron Rad.* **3**, 101–111.

Helliwell, J. R. (1992). *Macromolecular Crystallography with Synchrotron Radiation.* Cambridge University Press.

Helliwell, J. R., Habash, J., Cruickshank, D. W. J., Harding, M. M., Greenhough, T. J., Campbell, J. W., Clifton, I. J., Elder, M., Machin, P. A., Papiz, M. Z. & Zurek, S. (1989). *J. Appl. Cryst.* **22**, 483–497.

Hubbell, J. H. & Seltzer, S. M. (2004). *Tables of X-ray Mass Attenuation Coefficients and Mass Energy-Absorption Coefficients*, Version 1.4, http://physics.nist.gov/xaamdi (25 March 2005). National Institute of Standards and Technology, Gaithersburg, MD. Originally published as: NISTIR 5632, National Institute of Standards and Technology, Gaithersburg, MD, USA (1995).

Pilon, M. J., Schleicher, R. G., Moran, P. M. & Smith, S. B. Jr (1990). *Appl. Spectrosc.* **44**, 1613–1620.

Sims, G. R. (1994). *Principles of Charge Transfer Devices*, ch. 2, in *Charge-Transfer Devices in Spectroscopy*, edited by J. V. Sweedler, K. L. Ratzlaff and M. B. Denton. New York: Wiley.

Sims, G. R. & Denton, M. B. (1990). *Talanta*, **37**, 1–13.

Stoddard, B. L. & Farber, G. K. (1995). *Structure*, **3**, 991–996.

Strobel, H. R. & Heineman, W. R. (1989). *Chemical Instrumentation: A Systematic Approach*, 3rd ed. New York: John Wiley-Interscience.

Yamashita, A., Endo, M., Higashi, T., Nakatsu, T., Yamada, Y., Oda, J. & Kat, H. (2003). *Biochemistry*, **42**, 5566–5573.